JACS
JOURNAL OF THE AMERICAN CHEMICAL SOCIETY
pubs.acs.org/JACS
Article

Tuning Octahedral Tilting by Doping to Prevent Detrimental Phase Transition and Extend Carrier Lifetime in Organometallic Perovskites

Junwen Yin,[▽] Zhongfei Xu,[▽] Qi Hu,[▽] Gilberto Teobaldi, Li-Min Liu,* and Oleg V. Prezhdo*

Cite This: J. Am. Chem. Soc. 2023, 145, 5393−5399

ABSTRACT: As one of the most promising materials for next-generation solar cells, organometallic perovskites have attracted substantial fundamental and applied interest. Using first-principles quantum dynamics calculations, we show that octahedral tilting plays an important role in stabilizing perovskite structures and extending carrier lifetimes. Doping the material with (K, Rb, Cs) ions at the A-site enhances octahedral tilting and the stability of the system relative to unfavorable phases. The stability of doped perovskites is maximized for uniform distribution of the dopants. Conversely, aggregation of dopants in the system inhibits octahedral tilting and the associated stabilization. The simulations also indicate that with enhanced octahedral tilting, the fundamental band gap increases, the coherence time and nonadiabatic coupling decrease, and the carrier lifetimes are thus extended. Our theoretical work uncovers and quantifies the heteroatom-doping stabilization mechanisms, opening up new avenues to enhancing the optical performance of organometallic perovskites.

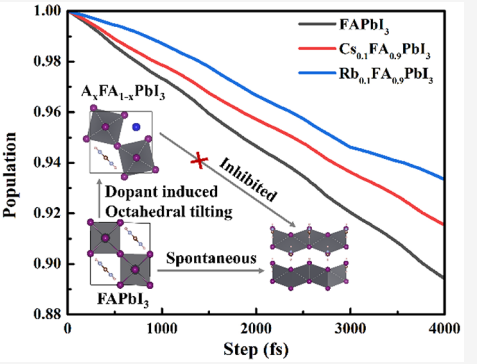

1. INTRODUCTION

Due to their exciting optoelectronic properties and low-cost preparation and deposition protocols, ABX_3 hybrid organic−inorganic pervoskites (HOIPs) hold great promise for future, scalable solar cells and photovoltaics devices. The certified efficiency of HOIP solar-cells has seen very rapid improvements, recently reaching figures as high as 25.2%, which is competitive against conventional Si-based solar cells.[1−7] The biggest hurdle for commercial uptake of HOIP solar cells remains the instability of the HOIP material under working conditions.[8−15] For this barrier to be overcome and step-change developments in perovskite solar cells to be possible, a deeper understanding of HOIPs' instabilities is necessary.[16] As the archetypal HOIPs, methylammonium (MA) lead halide ($CH_3NH_3PbX_3$) and formamidinium (FA) lead halide ($CH(NH_2)_2PbX_3$) exhibit high light absorption coefficient and long charge carrier diffusion lengths.[17−24] However, the instability of both structures under light, heat, and moisture has so far hindered their large-scale uptake for practical applications.

For $MAPbX_3$, the low calculated formation energy (0.11−0.14 eV per unit cell) leads to intrinsic thermal instability at working environment.[22] In addition, $MAPbX_3$ suffers from a hexagonal-to-cubic phase transition at about 56 °C, which can result in large volume changes and accelerated mechanical deformations.[25] As for $FAPbX_3$, the substitution of MA with FA has been shown to effectively improve the thermal stability.[17,18,26,27] $FAPbX_3$ has been observed to remain unbleached for more than 60 min after being heated to 150 °C, in contrast to $MAPbI_3$ that is conversely bleached within 30 min.[17] In addition, $FAPbI_3$ with fully vertex connected PbI_6 octahedra has an optical band gap of 1.47 eV, smaller than that of $MAPbI_3$, thus extending the optical absorption into the near-infrared region.[27] Despite its improved thermal stability and optical absorption, $FAPbI_3$ does present challenges in terms of structural stability and resilience of its photovoltaics effect as a result of its well-documented perovskite to nonperovskite (α-to-δ) transition.[28−32]

The unwanted α-to-δ transition takes place at room temperature, and several studies have explored strategies to stabilize the perovskite (α) phase of $FAPbI_3$. Zheng et al. improved the phase stability of $FAPbI_3$ by introducing heterogeneous dopants to realize strain relaxation.[33] Sargent and co-workers succeeded in increasing the stability of halide perovskite solar cells by suppressing atomic vacancies via incorporation of isovalent small ions.[16] However, the intrinsic mechanism of the phase transition remains unsolved, prompting further investigations toward atomic understanding of the cubic phase stabilization as well as strategies to enhance it.

Received: December 21, 2022
Published: February 21, 2023

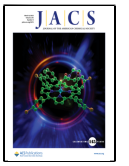

https://doi.org/10.1021/jacs.2c13593
J. Am. Chem. Soc. 2023, 145, 5393−5399

To this end, here we combine density functional theory (DFT), DFT molecular dynamics (DFT-MD), and non-adiabatic molecular dynamics (NAMD) simulations to provide a holistic theoretical investigation on the $FAPbI_3$ perovskite system and the interplay between its structural stability and optoelectronics properties. The DFT calculated internal energy of $FAPbI_3$ as a function of its octahedral tilting confirms that octahedral tilting can effectively lower the internal energy of perovskite structures. Notably, tilting is computed also to be effective in further reducing the internal energy difference between the δ and α phases. We furthermore investigate the effects of heavy alkali-metal dopants (K, Rb, Cs) at the perovskite A-site on the structure and internal energy of different $A_xFA_{1-x}PbI_3$ derivatives. It is found that the asymmetric distribution of the FA-molecules and A-dopants introduces spontaneous octahedral tilting into the cubic system and decreases its internal energy, thus hindering the phase transition between the cubic and hexagonal phases. Further simulations of the $A_xFA_{1-x}PbI_3$ systems reveals that the perovskite phase can be maximally stabilized by doping uniformly distributed heteroatoms. The doped $A_xFA_{1-x}PbI_3$ systems are additionally characterized in terms of electronic properties and carrier lifetime by means of NAMD calculations. It is shown that the considered dopants do not introduce gap states and can effectively extend the carrier lifetime.

2. RESULTS AND DISCUSSION

As shown in Figure 1, $FAPbI_3$ has an ABX_3 structure in which the A-, B-, and X-sites are occupied by FA, Pb, and I,

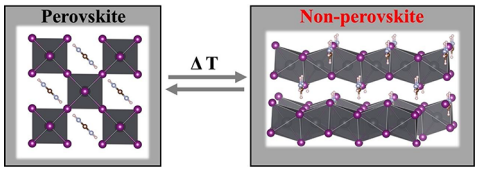

Figure 1. Phase transition diagram of $FAPbI_3$. The perovskite α phase of $FAPbI_3$ (left), which is the photoactive phase, exists at high temperature (>300 K). The nonperovskite δ phase of $FAPbI_3$ (right), which is the photoinactive phase, exists at low temperature (<300 K). A temperature (~300 K) triggered phase transition connects the two phases.

respectively. Upon cooling, $FAPbI_3$ undergoes a phase transition at about 300 K from a high-temperature α phase crystallized in the space group $Pm3m$ to a low-temperature δ phase with a $P63mc$ symmetry.[19] The structures of the α and δ phases of $FAPbI_3$ do not have a group−subgroup relationship, which implies a first-order character of the phase transition, and a complex pattern of sliding and twisting of organic molecules, lead, and iodide atoms. We initiate our investigation of the α-to-δ phase transition by comparing the internal energy of the two phases at 0 K. In the following, we refer to the internal energy difference between the α and δ phases as the energy difference ΔE. When the α phase takes the high-symmetry cubic structure, δ-$FAPbI_3$ is more stable than α-$FAPbI_3$ by about 0.41 eV. Such a calculated energy difference is consistent with the experimental observation that δ phase is the ground state at low temperature.

Different from the rigid face-sharing framework of the δ phase, the α phase presents a more flexible corner-sharing network, leading to the occurrence of a very complex energy landscape with different molecular distributions and distortions from the high-symmetry cubic structure. Herein, we set to investigate the influence of octahedral tilting on the internal energy of the perovskite structure. According to the Glazer notation, the octahedral tilting is noted as a linear combination of in-phase and out-of-phase rotations along the crystallographic axes.[34] For example, the $a^0b^+c^-$ labeling indicates one in-phase tilt along the [010] direction and one out-of-phase tilt along the [001] direction. As shown in Figure 2g, we take three different octahedral tilting patterns to obtain a representative energy surface of $FAPbI_3$.

We define the deviation from 90° of the intersection angle of neighboring PbI_6 octahedra (I−I−I) as the tilting angle. As shown in Figure 2a, if the intersection angle of neighboring PbI_6 octahedra is x, the tilting angle is unambiguously defined as $(90 - x)$. When the PbI_6 octahedral network is highly symmetric and the tilting angle is zero, the internal energy of the system is the highest. Conversely, the appearance of octahedral tilting decreases the internal energy of the system, as shown in Figure 2g. In contrast, for the nonperovskite hexagonal structure, the presence of face sharing PbI_6 octahedra prevents octahedral tilting and associated energy fluctuations. Due to the different tiltings possible in the cubic and hexagonal phases, enhancing such a structural deformation in the former can be very meaningfully targeted to reduce the energy difference between the two phases, toward hindering of the unwanted cubic to hexagonal transition (Figure 1). Moreover, heteroatom doping has been proposed as an effective approach to stabilize the perovskite structure, although the interplay between doping and octahedral tilting has so far remained largely overlooked.[16,29,30,32,33,36,37] To fill this gap and elucidate the interplay between heteroatom doping and octahedral tilting, in the following we investigate different hetero A-cation (K, Rb, Cs) doping of $FAPbI_3$, quantifying its effects on the octahedral tilting for the doped system.

As shown in Figure 2e, for pure cubic ABX_3 perovskite structures, the PbI_6 octahedra are uniformly surrounded by A-cations, which leads to 0° octahedral tilting angles. However, with the hetero A-cations doped into the lattice, the PbI_6 octahedra are surrounded by different A-cations, which results in nonzero octahedral tilting (Figure 2d). Figure S1 lists typical A-cations for ABX_3 systems in increasing order of their ionic radius. To gain insight into the origins of improved stability of hetero A-cation-doped $FAPbI_3$, we have calculated the optimized geometry and internal energy of three different systems ($Cs_{0.5}FA_{0.5}PbI_3$, $K_{0.5}FA_{0.5}PbI_3$, and $Rb_{0.5}FA_{0.5}PbI_3$). First, taking $Cs_{0.5}FA_{0.5}PbI_3$ as an example, the octahedral tilting of the α phase is clearly enhanced by the Cs dopants. However, in the hexagonal phase of $Cs_{0.5}FA_{0.5}PbI_3$, no obvious octahedral tilting is observed, due to the rigid face-sharing octahedral frameworks. For pure $FAPbI_3$, the energy difference between the cubic and hexagonal phases is 0.26 eV. For $Cs_{0.5}FA_{0.5}PbI_3$, the energy difference is reduced to 0.05 eV. It can thus be concluded that the α phase can be stabilized by doping A-cations (e.g., Cs) with an ionic radius smaller than FA's, as a result of an energetically beneficial, increased octahedral tilting in the system.

Next, we turn to discuss the effects of the radius difference between the A- and FA-cations. As shown above, stabilization of the α phase via Cs-doping at the A-sites originates from the increased octahedral tilting introduced by the presence of (Cs) dopants. Based on such octahedral tilting mechanism, we

https://doi.org/10.1021/jacs.2c13593
J. Am. Chem. Soc. 2023, 145, 5393−5399

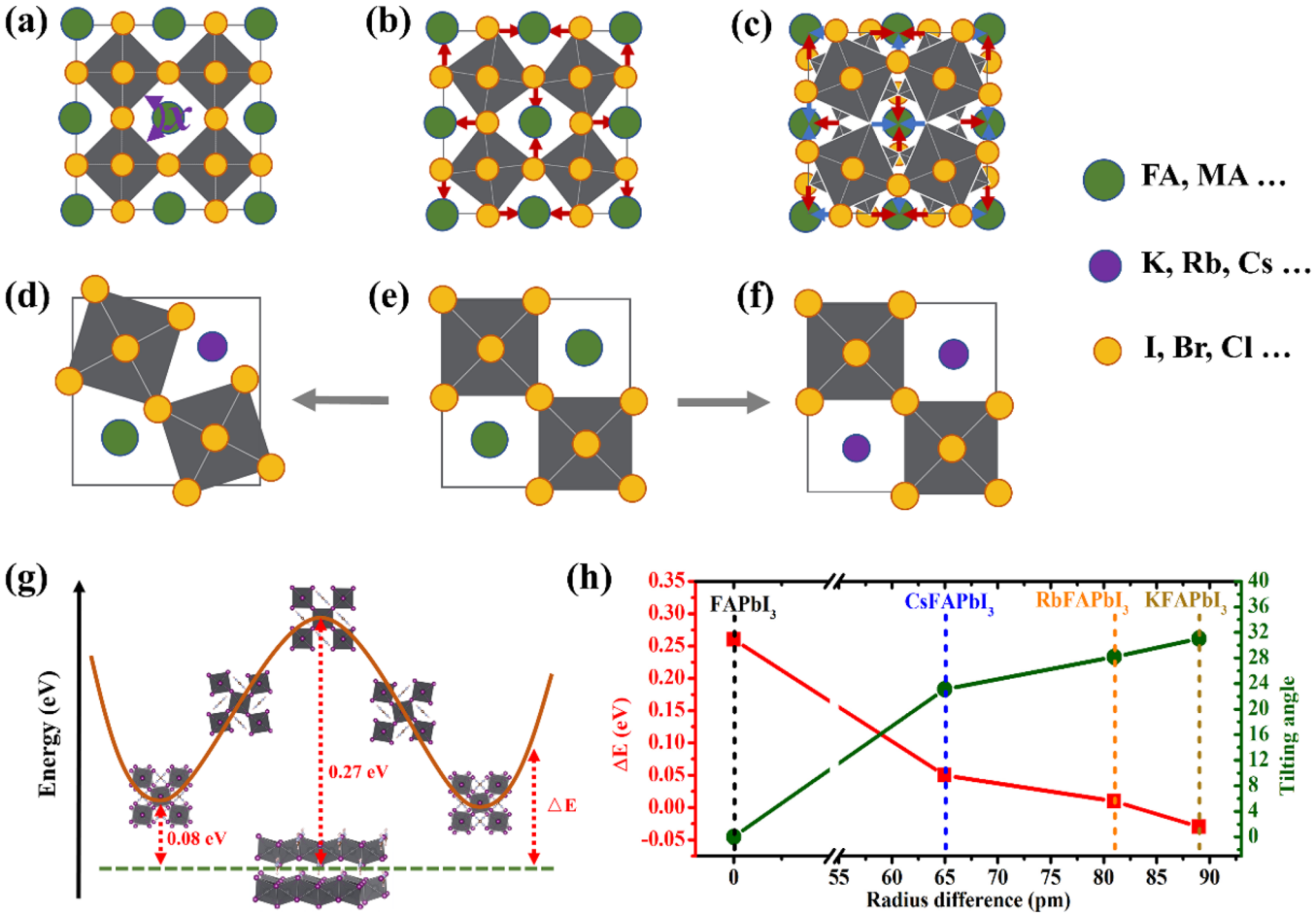

Figure 2. Schematic illustration of different octahedral tilting patterns in the pristine and heterodoped-doped materials, double-well potential energy surface associated with octahedral tilting in the perovskite (cubic) structure, and the calculated ΔE as a function of the A-dopant. (a−c) Octahedral tilting patterns in the perovskite (cubic) structure. (d−f) Illustration of spontaneous octahedral tilting introduced by heterodopants. (g) Energy difference (ΔE) between the α (perovskite, cubic) and δ (nonperovskite, hexagonal) phases and the other perovskite structures with different tilting angles. Typical tilting angles of 0°, 9.52°, and 25.26° were considered. (h) Calculated ΔE and tilting angle as functions of the ionic-radius difference between the pristine FA-cations and the A-dopants ($R_{FA} - R_A$, A-dopants are Cs, Rb, and K). The ionic radius information are taken from the Shannon radii data set.[35]

extend our investigation by further considering other alkali-metal dopants, such as K and Rb. As shown in Figure 2h, the octahedral tilting is strongly correlated with the ionic radius of the A-dopant. As the ionic radius for the A-cation becomes smaller, and its difference from the FA radius increases, the octahedral tilting angle in the doped perovskite also becomes larger. For example, the radius difference between Cs and FA is 65 pm, and the tilting angle in $Cs_{0.5}FA_{0.5}PbI_3$ is 23.11°. As the atomic radius of Rb (K) becomes smaller, leading to larger differences of 81 pm (89 pm) from the value for the FA-cation, the tilting angle systematically increases to 28.17° for $Rb_{0.5}FA_{0.5}PbI_3$ (31.02° for $K_{0.5}FA_{0.5}PbI_3$), with an ensuing reduction of the energy difference, thence stabilization of the α phase (Figure 2h). Notably, for K, the energy difference becomes slightly negative (−0.03 eV/unit cell), indicating that for this system the α phase is now energetically favored over the δ phase.

Although these calculated results indicate that replacement of the FA cation in $FaPbI_3$ by K, Cs, and Rb could improve the stability of the desired perovskite α phase, the aggregation of heterogeneous A-cations remains a potential big challenge. In this respect, we next explore the role of dopant distribution homogeneity for the stabilization of the α-phase. As shown in Figure 3a−c, we explore $Cs_xFA_{1-x}PbI_3$ (x = 0.11, 0.15, 0.19) with two different Cs distributions. Figure 3a−c, top, shows the system with Cs-aggregation, whereas Figure 3a−c, bottom, reports the system with homogeneously distributed Cs-dopants. It can be observed that homogeneous distribution of the Cs-dopant introduces the largest octahedral tilting in the system (represented in Figure 2d−e). Conversely, aggregation of Cs-dopants leads to very local distortion and effectively no octahedral tilting across most of the sample (represented in Figure 2e,f).

DFT calculated internal energies (Table 1) indicate that, only when the Cs-dopants are well-distributed in the framework, the octahedral tilting and the system stabilization are maximized. For different Cs-dopant concentrations ranging from 11% to 19%, the stabilization energy due to homogeneous distribution of the Cs-dopants is substantial, ranging from −0.02 to −0.06 eV per Cs-atom. Our results clearly suggest that, when doping heteroatoms into the system, the uniformity of the dopants should be as high as possible.

The electronic structure of the different Cs-doped $FAPbI_3$ systems is next considered to analyze systematically the effects of this inorganic dopant. As shown in Figure 3d,e, the calculated density of states for $Cs_{0.15}FA_{0.85}PbI_3$ for both

https://doi.org/10.1021/jacs.2c13593
J. Am. Chem. Soc. 2023, 145, 5393−5399

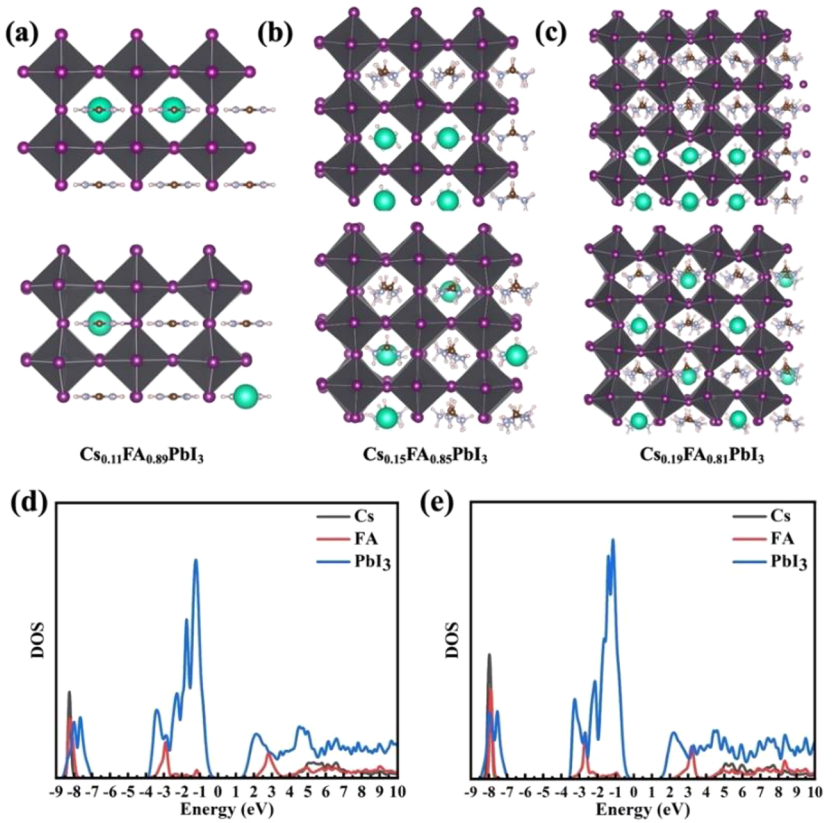

Figure 3. Effects of the hetero A-dopants on the electronic structure. (a–c) Aggregated-dispersed Cs-doped $FAPbI_3$ (top) and well-dispersed Cs-doped $FAPbI_3$ (bottom). (d) Density of states (DOS) for $Cs_{0.15}FA_{0.85}PbI_3$ with aggregated Cs-dopants. (e) DOS of $Cs_{0.15}FA_{0.85}PbI_3$ for well-dispersed Cs-dopants.

Table 1. Effects of the Heteroatom Distribution and Concentration on the Energy Stabilization of the α Phase for Aggregated and Well-Dispersed Cs-Dopants[a]

supercell size	3 × 3 × 2	3 × 3 × 3	4 × 4 × 4
formula	$Cs_{0.11}FA_{0.89}PbI_3$	$Cs_{0.15}FA_{0.85}PbI_3$	$Cs_{0.19}FA_{0.81}PbI_3$
$E_{aggregated}$ (eV)	0	0	0
$E_{well\text{-}dispersed}$ (eV)	−0.05	−0.24	−0.18
$E_{stabilization}$/Cs (eV)	−0.02	−0.06	−0.02

[a]Here, we define the total energy of system with aggregated Cs-dopant as zero. $E_{stabilization}$/Cs is the energy difference, normalized to the number of Cs-atoms, between the systems with aggregated and well-dispersed Cs-dopants.

homogeneous and inhomogeneous Cs-distributions turns out to be rather similar to that of the pristine, dopant-free $FAPbI_3$. No gap states are observed as the Cs electronic states are relatively deep in the valence band. These results show that Cs doping can stabilize the perovskite α structure of $FAPbI_3$ without introducing defect states, which are detrimental to the optoelectronic performance of the system.[38]

In the final part of the contribution, we analyze and discuss charge recombination in $FAPbI_3$ with enhanced octahedral tilting introduced by hetero A-cations (Rb and Cs). Previous reports demonstrate that octahedral tilting in undoped samples decreases the nonadiabatic couplings (NACs) and coherence time in HOIPs, further extending the carrier lifetimes.[39,40] Here, we investigate the role of the dopant-induced octahedral tilting for the carrier lifetimes in A-doped HOIPs. We carried out 6 ps DFT-MD simulations and NAMD calculations for both $Cs_{0.1}FA_{0.9}PbI_3$ and $Rb_{0.1}FA_{0.9}PbI_3$. Figure 4a shows the electron–hole recombination dynamics by focusing on the decay of the first excited-state population for the two systems. The recombination times are obtained by fitting the exponential decay, $f(t) = \exp(-t/\tau) \approx 1 - t/\tau$, yielding τ = 0.047 ns for the Cs-doped system and τ = 0.06 ns for the Rb-doped one. The results for both systems indicate noticeably increased (+27% and +62%) recombination times t relative to pristine $FAPbI_3$ (0.037 ns).

To understand the origin of the increased carrier lifetimes for $Cs_{0.1}FA_{0.9}PbI_3$ and $Rb_{0.1}FA_{0.9}PbI_3$, we investigate and quantify the effects of (A-cation induced) octahedral tilting on the band gap energies and NACs. According to the gap law, carrier lifetimes grow as the gap increases, with band gap opening distortions contributing to extended electron–hole recombination times.[41] As it can be seen in the projected density of states of $FAPbI_3$ in Figure 4c,d, A-dopant-induced octahedral tilting has a notable effect on the band gap energy, increasing the latter from 1.32 to 1.65 eV. Such a phenomenon results from an decreased overlap between I 5p and Pb 6s states due to the tilting of the PbI_6 octahedra.[41] The octahedral tilting of $Rb_{0.1}FA_{0.9}PbI_3$ is more marked than that of $Cs_{0.1}FA_{0.9}PbI_3$ (Figure 4b), resulting in larger band gap fluctuations and a longer calculated carrier recombination

https://doi.org/10.1021/jacs.2c13593
J. Am. Chem. Soc. 2023, 145, 5393–5399

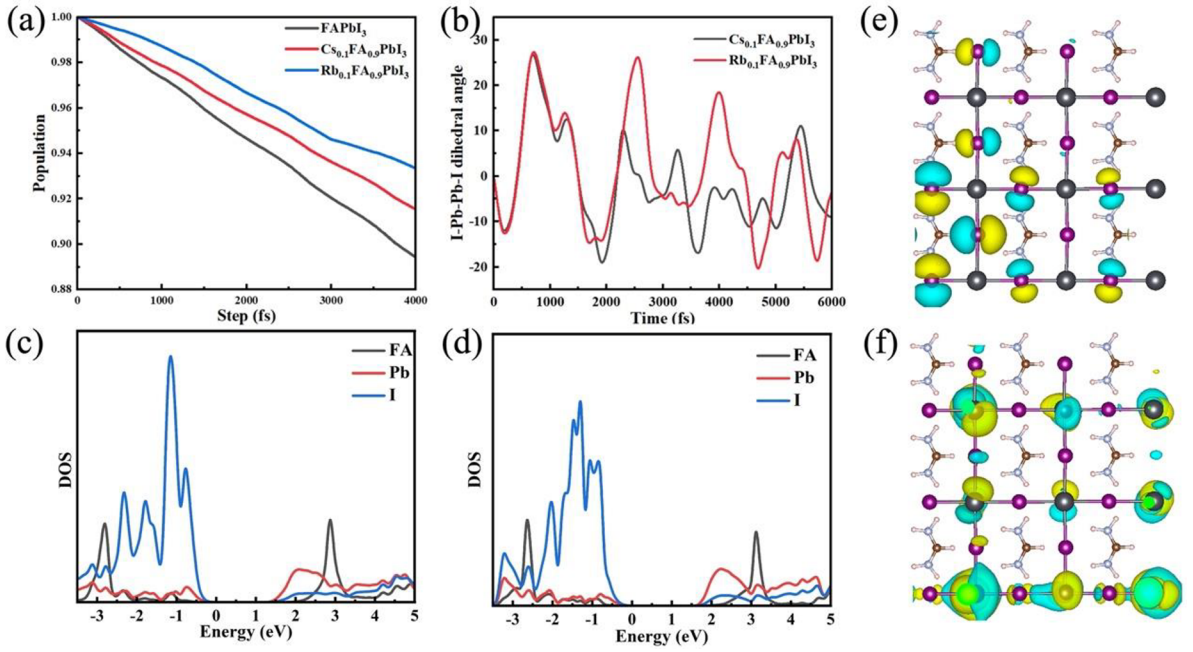

Figure 4. (a) Excited-state population decay in $Cs_{0.1}FA_{0.9}I_3$ and $Rb_{0.1}FA_{0.9}I_3$ at 300 K. (b) Time-evolution of the I−Pb−Pb−I dihedral angle during the DFT-MD trajectory. (c and d) Density of states (DOS) for $FAPbI_3$ with (c) $a^0b^0c^0$ and (d) $a^0b^+c^-$ octahedral patterns. (e and f) HOMO and LUMO charge densities for $FAPbI_3$.

time of for the Rb-doped system with respect to the results for the Cs-doped one.

We next turn to the analysis of NACs that influence significantly the recombination process. Generally, to increase the carrier lifetime, the overlap of the HOMO and LUMO wave functions and the gradient with respect to nuclear dispacements, $\langle\varphi_j|\nabla_R|\varphi_k\rangle$, should be reduced. As shown in Figure 4e,f, in $FAPbI_3$, the HOMO is dominated by iodine and the LUMO by lead atoms. However, in hetero A-cation-doped $FAPbI_3$, the stronger octahedral tilting results in a longer Pb−I distance, reducing the HOMO−LUMO overlap (Figure S3). It follows that the enhanced octahedral tilting, thence reduced NACs, brought about by hetero A-cation dopants, should be highly effective in increasing the carrier lifetimes in the-doped systems.

3. CONCLUSION

Our work provides new theoretical guidelines for enhancing the stability and optical performance of A-cation-doped, ABX_3 perovskite structures. It is shown that octahedral tilting plays an important role in stabilizing perovskite structures as well as in extending the associated carrier lifetime. By doping hetero A-cations into the system, spontaneous octahedral tilting is introduced, which lowers the internal energy of the doped ABX_3 structures. We have furthermore shown that homogeneous dispersion of the dopants is crucial for introduction of the maximum level of octahedral tilting and stabilization of the system, with clustering of dopants into an inhomogeneous distribution being highly ineffective on both accounts. Finally, we have quantified the effects of octahedral tilting and heteroatom doping on the electronic structure of $FAPbI_3$. It is shown that A-cation doping can stabilize the perovskite structures without losing the optimal band gap for photovoltaic performance. Additional NAMD calculations confirm that octahedral tilting can effectively extend carrier lifetimes. We expect these findings and insights to benefit the ongoing development of new strategies to realize the full potential of perovskite-based optical electronics for stable, commercially viable devices.

■ ASSOCIATED CONTENT

Supporting Information

The Supporting Information is available free of charge at https://pubs.acs.org/doi/10.1021/jacs.2c13593.

Discussion of calculation methods and figures of ionic radius of different A-cations, structures of the 3 × 3 × 1 supercell of $Cs_{0.1}FA_{0.9}PbI_3$ and $Rb_{0.1}FA_{0.9}PbI_3$, and HOMO and LUMO of $Cs_{0.1}FA_{0.9}PbI_3$ and $Rb_{0.1}FA_{0.9}PbI_3$ (PDF)

■ AUTHOR INFORMATION

Corresponding Authors

Li-Min Liu − *School of Physics, Beihang University, Beijing 100083, China;* orcid.org/0000-0003-3925-5310; Email: liminliu@buaa.edu.cn

Oleg V. Prezhdo − *Departments of Chemistry, and Physics and Astronomy, University of Southern California, Los Angeles, California 90089, United States;* orcid.org/0000-0002-5140-7500; Email: prezhdo@usc.edu

Authors

Junwen Yin − *School of Physics, Beihang University, Beijing 100083, China; Beijing Compuational Science Research Center, Beijing 100081, China*

Zhongfei Xu − *College of Environmental Science and Engineering, North China Electric Power University, Beijing 102206, China*

Qi Hu − *School of Physics, Beihang University, Beijing 100083, China*

Gilberto Teobaldi − *Scientific Computing Department, STFC UKRI, Rutherford Appleton Laboratory, Didcot OX11 0QX, United Kingdom; School of Chemistry, University of*

https://doi.org/10.1021/jacs.2c13593
J. Am. Chem. Soc. 2023, 145, 5393−5399

Southampton, Highfield, Southampton SO17 1BJ, United Kingdom; orcid.org/0000-0001-6068-6786

Complete contact information is available at: https://pubs.acs.org/10.1021/jacs.2c13593

Author Contributions

[V]J.Y., Z.X., and Q.H. contributed equally to this work.

Notes

The authors declare no competing financial interest.

■ ACKNOWLEDGMENTS

This work was financially supported by the National Key Research and Development Program of China (No. 2022YFB4200500) and the National Natural Science Foundation of China (Nos. 52225308,11974037, and 12204168). G.T. and L.-M.L. acknowledge support by the Royal Society Newton Advanced Fellowship scheme (grant No. NAF \R1\180242). O.V.P. acknowledges support of the US National Science Foundation (grant No. CHE-2154367). The authors are grateful to the Beihang HPC and Tianhe2-JK for generous grants of computer time.

■ REFERENCES

(1) Yoo, J. J.; Seo, G.; Chua, M. R.; Park, T. G.; Lu, Y.; Rotermund, F.; Kim, Y.-K.; Moon, C. S.; Jeon, N. J.; Correa-Baena, J.-P.; et al. Efficient Perovskite Solar Cells via Improved Carrier Management. *Nature* **2021**, *590* (7847), 587−593.

(2) Burschka, J.; Pellet, N.; Moon, S.-J.; Humphry-Baker, R.; Gao, P.; Nazeeruddin, M. K.; Gratzel, M. Sequential Deposition as a Route to High-Performance Perovskite-Sensitized Solar Cells. *Nature* **2013**, *499* (7458), 316−320.

(3) Stranks, S. D.; Snaith, H. J. Metal-Halide Perovskites for Photovoltaic and Light-Emitting Devices. *Nat. Nanotechnol.* **2015**, *10* (5), 391−402.

(4) Im, J.-H.; Jang, I.-H.; Pellet, N.; Grätzel, M.; Park, N.-G. Growth of $CH_3NH_3PbI_3$ Cuboids with Controlled Size for High-Efficiency Perovskite Solar Cells. *Nat. Nanotechnol.* **2014**, *9* (11), 927−932.

(5) Im, J.-H.; Lee, C.-R.; Lee, J.-W.; Park, S.-W.; Park, N.-G. 6.5% Efficient Perovskite Quantum-Dot-Sensitized Solar Cell. *Nanoscale* **2011**, *3* (10), 4088−4093.

(6) Hao, F.; Stoumpos, C. C.; Liu, Z.; Chang, R. P. H.; Kanatzidis, M. G. Controllable Perovskite Crystallization at a Gas−Solid Interface for Hole Conductor-Free Solar Cells with Steady Power Conversion Efficiency over 10%. *J. Am. Chem. Soc.* **2014**, *136* (46), 16411−16419.

(7) Kojima, A.; Teshima, K.; Shirai, Y.; Miyasaka, T. Organometal Halide Perovskites as Visible-Light Sensitizers for Photovoltaic Cells. *J. Am. Chem. Soc.* **2009**, *131* (17), 6050−6051.

(8) Wang, Z.; Lin, Q.; Chmiel, F. P.; Sakai, N.; Herz, L. M.; Snaith, H. J. Efficient Ambient-Air-Stable Solar Cells with 2D−3D Heterostructured Butylammonium-Caesium-Formamidinium Lead Halide Perovskites. *Nat. Energy* **2017**, *2* (9), 17135.

(9) Tsai, H.; Nie, W.; Blancon, J.-C. High-Efficiency Two-Dimensional Ruddlesden−Popper Perovskite Solar Cells. *Nature* **2016**, *536* (7616), 312−316.

(10) Arora, N.; Dar, M. I.; Hinderhofer, A.; Pellet, N.; Schreiber, F.; Zakeeruddin, S. M.; Gratzel, M. Perovskite Solar Cells with CuSCN Hole Extraction Layers Yield Stabilized Efficiencies Greater than 20%. *Science* **2017**, *358* (6364), 768−771.

(11) You, J.; Meng, L.; Song, T. B. Improved Air Stability of Perovskite Solar Cells via Solution-Processed Metal Oxide Transport Layers. *Nat. Nanotechnol.* **2015**, *11* (1), 75−81.

(12) Hou, Y.; Du, X.; Scheiner, S. A Generic Interface to Reduce the Efficiency-Stability-Cost Gap of Perovskite Solar Cells. *Science* **2017**, *358* (6367), 1192−1197.

(13) Christians, J. A.; Schulz, P.; Tinkham, J. S. Tailored Interfaces of Unencapsulated Perovskite Solar Cells for > 1,000 h Operational Stability. *Nat. Energy* **2018**, *3* (1), 68−74.

(14) Yang, Y.; You, J. Make Perovskite Solar Cells Stable. *Nature* **2017**, *544* (7649), 155−156.

(15) Zhao, P.; Kim, B. J.; Jung, H. S. Passivation in Perovskite Solar Cells: A Review. *Mater. Today Energy* **2018**, *7*, 267−286.

(16) Saidaminov, M. I.; Kim, J.; Jain, A.; Quintero-Bermudez, R.; Tan, H.; Long, G.; Tan, F.; Johnston, A.; Zhao, Y.; Voznyy, O.; Sargent, E. H. Suppression of Atomic Vacancies via Incorporation of Isovalent Small Ions to Increase the Stability of Halide Perovskite Solar Cells in Ambient Air. *Nat. Energy 2018 3:8* **2018**, *3* (8), 648−654.

(17) Eperon, G. E.; Stranks, S. D.; Menelaou, C.; Johnston, M. B.; Herz, L. M.; Snaith, H. J. Formamidinium Lead Trihalide: A Broadly Tunable Perovskite for Efficient Planar Heterojunction Solar Cells. *Energy Environ. Sci.* **2014**, *7* (3), 982−988.

(18) Zhumekenov, A. A.; Saidaminov, M. I.; Haque, M. A.; Alarousu, E.; Sarmah, S. P.; Murali, B.; Dursun, I.; Miao, X.-H.; Abdelhady, A. L.; Wu, T.; et al. Formamidinium Lead Halide Perovskite Crystals with Unprecedented Long Carrier Dynamics and Diffusion Length. *ACS Energy Lett.* **2016**, *1* (1), 32−37.

(19) Weller, M. T.; Weber, O. J.; Frost, J. M.; Walsh, A. Cubic Perovskite Structure of Black Formamidinium Lead Iodide, α-$[HC(NH_2)_2]PbI_3$, at 298 K. *J. Phys. Chem. Lett.* **2015**, *6* (16), 3209−3212.

(20) Han, Q.; Bae, S.-H.; Sun, P.; Hsieh, Y.-T.; Yang, Y.; Rim, Y. S.; Zhao, H.; Chen, Q.; Shi, W.; Li, G.; Yang, Y. Single Crystal Formamidinium Lead Iodide ($FAPbI_3$): Insight into the Structural, Optical, and Electrical Properties. *Adv. Mater.* **2016**, *28* (11), 2253−2258.

(21) Fabini, D. H.; Stoumpos, C. C.; Laurita, G.; Kaltzoglou, A.; Kontos, A. G.; Falaras, P.; Kanatzidis, M. G.; Seshadri, R. Reentrant Structural and Optical Properties and Large Positive Thermal Expansion in Perovskite Formamidinium Lead Iodide. *Angew. Chem., Int. Ed.* **2016**, *128* (49), 15618−15622.

(22) Conings, B.; Drijkoningen, J.; Gauquelin, N.; Babayigit, A.; D'Haen, J.; D'Olieslaeger, L.; Ethirajan, A.; Verbeeck, J.; Manca, J.; Mosconi, E.; et al. Intrinsic Thermal Instability of Methylammonium Lead Trihalide Perovskite. *Adv. Energy Mater.* **2015**, *5* (15), 1500477.

(23) Brivio, F.; Frost, J. M.; Skelton, J. M.; Jackson, A. J.; Weber, O. J.; Weller, M. T.; Goñi, A. R.; Leguy, A. M. A.; Barnes, P. R. F.; Walsh, A. Lattice Dynamics and Vibrational Spectra of the Orthorhombic, Tetragonal, and Cubic Phases of Methylammonium Lead Iodide. *Phys. Rev. B* **2015**, *92* (14), 144308.

(24) Franssen, W. M. J.; van Es, S. G. D.; Dervişoğlu, R.; de Wijs, G. A.; Kentgens, A. P. M. Symmetry, Dynamics, and Defects in Methylammonium Lead Halide Perovskites. *J. Phys. Chem. Lett.* **2017**, *8* (1), 61−66.

(25) Baikie, T.; Fang, Y.; Kadro, J. M.; Schreyer, M.; Wei, F.; Mhaisalkar, S. G.; Graetzel, M.; White, T. J. Synthesis and Crystal Chemistry of the Hybrid Perovskite $(CH_3NH_3)PbI_3$ for Solid-State Sensitised Solar Cell Applications. *J. Mater. Chem. A* **2013**, *1* (18), 5628−5641.

(26) Pang, S.; Hu, H.; Zhang, J.; Lv, S.; Yu, Y.; Wei, F.; Qin, T.; Xu, H.; Liu, Z.; Cui, G. $NH_2CH{=}NH_2PbI_3$: An Alternative Organolead Iodide Perovskite Sensitizer for Mesoscopic Solar Cells. *Chem. Mater.* **2014**, *26* (3), 1485−1491.

(27) Amat, A.; Mosconi, E.; Ronca, E.; Quarti, C.; Umari, P.; Nazeeruddin, M. K.; Grätzel, M.; de Angelis, F. Cation-Induced Band-Gap Tuning in Organohalide Perovskites: Interplay of Spin−Orbit Coupling and Octahedra Tilting. *Nano Lett.* **2014**, *14* (6), 3608−3616.

(28) Binek, A.; Hanusch, F. C.; Docampo, P.; Bein, T. Stabilization of the Trigonal High-Temperature Phase of Formamidinium Lead Iodide. *J. Phys. Chem. Lett.* **2015**, *6* (7), 1249−1253.

(29) Jeon, N. J.; Noh, J. H.; Yang, W. S.; Kim, Y. C.; Ryu, S.; Seo, J.; Seok, S. il. Compositional Engineering of Perovskite Materials for High-Performance Solar Cells. *Nature* **2015**, *517* (7535), 476−480.

(30) Lee, J.; Kim, D.; Kim, H.; Seo, S.; Cho, S. M.; Park, N. Formamidinium and Cesium Hybridization for Photo-and Moisture-stable Perovskite Solar Cell. *Adv. Energy Mater.* **2015**, *5* (20), 1501310.
(31) Leyden, M. R.; Lee, M. v; Raga, S. R.; Qi, Y. Large Formamidinium Lead Trihalide Perovskite Solar Cells Using Chemical Vapor Deposition with High Reproducibility and Tunable Chlorine Concentrations. *J. Mater. Chem. A* **2015**, *3* (31), 16097−16103.
(32) McMeekin, D. P.; Sadoughi, G.; Rehman, W.; Eperon, G. E.; Saliba, M.; Hörantner, M. T.; Haghighirad, A.; Sakai, N.; Korte, L.; Rech, B.; et al. A Mixed-Cation Lead Mixed-Halide Perovskite Absorber for Tandem Solar Cells. *Science* **2016**, *351* (6269), 151−155.
(33) Zheng, X.; Wu, C.; Jha, S. K.; Li, Z.; Zhu, K.; Priya, S. Improved Phase Stability of Formamidinium Lead Triiodide Perovskite by Strain Relaxation. *ACS Energy Lett.* **2016**, *1* (5), 1014−1020.
(34) Glazer, A. M. The Classification of Tilted Octahedra in Perovskites. *Acta Crystallogr.* **1972**, *28* (11), 3384−3392.
(35) Shannon, R. D. Revised Effective Ionic Radii and Systematic Studies of Interatomic Distances in Halides and Chalcogenides. *Acta Crystallogr.* **1976**, *32* (5), 751−767.
(36) Dang, H. X.; Wang, K.; Ghasemi, M.; Tang, M. C.; de Bastiani, M.; Aydin, E.; Dauzon, E.; Barrit, D.; Peng, J.; Smilgies, D. M.; de Wolf, S.; Amassian, A. Multi-Cation Synergy Suppresses Phase Segregation in Mixed-Halide Perovskites. *Joule* **2019**, *3* (7), 1746−1764.
(37) Syzgantseva, O. A.; Saliba, M.; Grätzel, M.; Rothlisberger, U. Stabilization of the Perovskite Phase of Formamidinium Lead Triiodide by Methylammonium, Cs, and/or Rb Doping. *J. Phys. Chem. Lett.* **2017**, *8* (6), 1191−1196.
(38) Tong, C. J.; Li, L.; Liu, L. M.; Prezhdo, O. V. Synergy between Ion Migration and Charge Carrier Recombination in Metal-Halide Perovskites. *J. Am. Chem. Soc.* **2020**, *142* (6), 3060−3068.
(39) Shi, R.; Fang, Q.; Vasenko, A. S.; Long, R.; Fang, W. H.; Prezhdo, O. V. Structural Disorder in Higher-Temperature Phases Increases Charge Carrier Lifetimes in Metal Halide Perovskites. *J. Am. Chem. Soc.* **2022**, *144* (41), 19137−19149.
(40) Li, W.; She, Y.; Vasenko, A. S.; Prezhdo, O. V. Ab Initio Nonadiabatic Molecular Dynamics of Charge Carriers in Metal Halide Perovskites. *Nanoscale* **2021**, *13* (23), 10239−10265.
(41) Englman, R.; Jortner, J. The Energy Gap Law for Non-Radiative Decay in Large Molecules. *J. Lumin.* **1970**, *1*−*2* (C), 134−142.

https://doi.org/10.1021/jacs.2c13593
J. Am. Chem. Soc. 2023, 145, 5393−5399